



**HAL**  
open science

# Modeling cell membrane electrodeformation by alternating electric fields

Elias Sabri, Christian Brosseau

► **To cite this version:**

Elias Sabri, Christian Brosseau. Modeling cell membrane electrodeformation by alternating electric fields. *Physical Review E*, 2021, 104 (3), pp.034413. 10.1103/physreve.104.034413 . hal-04194017


**HAL Id: hal-04194017**

**<https://hal.science/hal-04194017v1>**

Submitted on 1 Sep 2023

**HAL** is a multi-disciplinary open access archive for the deposit and dissemination of scientific research documents, whether they are published or not. The documents may come from teaching and research institutions in France or abroad, or from public or private research centers.

L'archive ouverte pluridisciplinaire **HAL**, est destinée au dépôt et à la diffusion de documents scientifiques de niveau recherche, publiés ou non, émanant des établissements d'enseignement et de recherche français ou étrangers, des laboratoires publics ou privés.

**Modeling cell membrane electrodeformation by alternating electric fields**E. Sabri and C. Brosseau <sup>\*</sup>*Univ Brest, CNRS, Lab-STICC, CS 93837, 6 avenue Le Gorgeu, 29238 Brest Cedex 3, France* (Received 19 April 2021; revised 3 August 2021; accepted 13 August 2021; published 22 September 2021)

With the aim of characterizing and gaining insight into the frequency response of cells suspended in a fluid medium and deformed with a controlled alternating electric field, a continuum-based analysis is presented for modeling electrodeformation (ED) via Maxwell stress tensor (MST) calculation. Our purpose here is to apply this approach to explain the fact that the electric field anisotropy and electrical conductivity ratio  $\Lambda$  of the cytoplasm and the extracellular medium significantly impact the MST exerted on the cytoplasm-membrane interface. One important finding is that the modulation of electrical cues and MST force by the frequency of the applied electric field provides an extremely rich tool kit for manipulating cells. We show the extreme sensitivity of proximity-induced capacitive coupling arising concomitantly when the magnitude of the MST increases as the distance between cells is decreased and the spatial anisotropy becomes important. Moreover, our model highlights the strongly localized character of the electrostatic field effect emanating from neighboring cells and suggests the possibility of exploiting cell distribution as a powerful tool to engineer the functional performance of cell assemblies by controlling ED and capacitive coupling. We furthermore show that frequency has a significant impact on the attenuation-amplification transition of MST, suggesting that shape anisotropy has a much weaker influence on ED of the cell membrane compared to the anisotropy induced by the orientation angle itself.

DOI: [10.1103/PhysRevE.104.034413](https://doi.org/10.1103/PhysRevE.104.034413)**I. INTRODUCTION AND MOTIVATION**

Growing interest in exploring electrodeformation (ED) of various soft material structures (including biological cells, liposomes, and giant unilamellar vesicles) derives, in part, from the potential to exploit advanced three-dimensional (3D) designs in emergent technologies, from biomedical devices to microfluidics and electromechanical soft components [1]. However, due to fragility and ultras-small dimensions (of around 5 nm thickness for cell membrane), biological cells are highly susceptible to undergoing irreversible mechanical deformation that severely limits their biological and chemical functions under extreme conditions involving electrical and mechanical force. Equally important, these general physical principles based on classical electrodynamics and mechanics, in conjunction with numerical methods, can be of considerable value in the interpretation of experimental results.

When an exogenous electric field with frequency  $\nu$  is applied to a biological cell a redistribution of internal charges with respect to the field lines takes place, i.e., relaxation. Models of the causal interaction between AC electric fields and ions or biomolecules of the cell show that there are different types of relaxation, which define material properties. In the range of frequencies which is of interest in this study, the changes in permittivity along the relaxation spectrum are divided into two main relaxation regions, namely,  $\alpha$  and  $\beta$ . The slow  $\alpha$  relaxation is associated with tangential flow of ions across membrane surfaces (100 Hz to a few kHz) which causes a surface electrical current. The  $\beta$  relaxation accounts for the relaxation of large biomolecules and for the accumula-

tion of electrical charge at cell membrane interfaces due to the Maxwell-Wagner-Sillars effect (a few kHz to several MHz), i.e., polarization due to the mismatch of the electrical properties at the cell membrane-external medium interfaces [2–4]. While ED models of cells under various electric field excitations were explored in [5–8] and more recently considered in [9–16], there are few, if any, reports of the electric field anisotropy and electrical conductivity ratio  $\Lambda = \sigma_c/\sigma_e$  of the cytoplasm  $\sigma_c$  and the extracellular medium (ECM)  $\sigma_e$  on the ED force distribution induced by the local transmembrane potential (TMP).

For present purposes, we start with a brief discussion of the basic concepts by considering the TMP and constraints associated with the core-shell geometry of cell and scales in theory, i.e., a dielectric nanometric membrane surrounded by conducting cytoplasm and ECM. Here, we consider a TMP smaller than the critical membrane breakdown voltage at which electroporation (a distinct problem of the current analysis) occurs, i.e., 1 V which is usually regarded as a phenomenological estimate for the electroporation threshold [17–19]. Furthermore, we refer to  $\nu_\alpha$  and  $\nu_\beta$  as the characteristic modes related to membrane surface currents and Maxwell-Wagner-Sillars polarization, respectively. If we instead consider that  $\nu > \nu_\beta$  the membrane is permeable to the electric field lines. Therefore, if  $\Lambda > 1$ , the cell is more polarizable than the ECM. The opposite limit,  $\nu < \nu_\alpha$ , occurs when the cell behaves as a dielectric having low losses (low conductivity), thus limiting the polarization of the intracellular medium. Since membrane charging occurs very rapidly compared to the oscillation timescale of the electric field [1,4], the electric field consequently remains confined in the ECM. On the contrary, if the cell is less polarizable than the medium, the electric field will essentially remain confined. The ECM

<sup>\*</sup>brosseau@univ-brest.fr

becomes more polarizable than the cell. Furthermore, in [9] the analysis of the excess ED force for a pair of cells and its counterpart for a single reference cell allows us to determine a separation distance-orientation angle diagram providing evidence of a separation distance beyond which the electrostatic interactions between a pair of biological cells become inconsequential for the ED.

In this study we seek to improve our theoretical understanding of the elastic membrane ED of a reference cell in close proximity of a neighboring cell under alternating electric field excitation by exploiting the anisotropic perturbation of the local electric field distribution. We also seek to unravel the role of frequency in modulating the attenuation-amplification transition of ED force which has not been fully considered in the literature. It is important to explore such possibilities and possible means to distinguish among these and other models so we can eventually learn the true nature of ED in cell assemblies. The Supplemental Material [20] contains the material properties of actual cells which have been deduced from consolidated literature data and describes additional results.

## II. NUMERICAL FORMULATION

Based on these motivations and observations, we consider a pair of cells in close proximity. The resulting setup is sketched in Fig. 1.

To reduce the computational complexities, we have only considered two-dimensional (2D) geometries. However, the models presented in this study can be easily extended to 3D objects. More specifically, two 2D square shaped configurations are designed (single-cell and two-cell, respectively) with, respectively, three and five subdomains [9]. The core-shell model of a biological cell, e.g., Ref. [2], serves as the basis from which we constructed our model that best aligns with our purpose. In Fig. 1, the single-cell model represents the reference cell. In the two-cell model, we consider a pair of cells suspended in a square domain and in close proximity (Fig. 1), where  $h$  is the dimension along the  $x$  and  $y$  directions, respectively. This dimension is found to be sufficiently large to have nonzero interactions between the periodic images of the lattice.

Numerical procedures to solve the continuum electrical and mechanical equations at first require a discretization. A 2D mesh was assembled using the COMSOL 5.5 software [21]. There was a total of 15 659 nodes and 31 256 elements in the mesh of the single-cell system and 30 576 nodes and 61 090 elements in the mesh of the two-cell system. Simulations are performed via a cluster computer [262 GB RAM, Intel Xeon 2.2 GHz (48 CPUs) processor]. Our results are based on a two-stage algorithm solving a set of equations in each domain of the simulated system, whose first stage is based on the calculation of the electrical part of the simulation via the following set of equations:  $\nabla \cdot \mathbf{J} = Q$ ,  $\mathbf{J} = \sigma \mathbf{E} + 2\pi i\nu \mathbf{D}$ ,  $\mathbf{E} = -\nabla V$ , and  $\mathbf{T} = \varepsilon \varepsilon_0 (\mathbf{E} \times \mathbf{E} - \frac{1}{2} \mathbf{E}^2)$ , where  $\mathbf{J}$ ,  $\mathbf{T}$ ,  $\mathbf{E}$ ,  $\mathbf{D}$ ,  $\sigma$ ,  $\varepsilon$ ,  $V$ , and  $Q$  account, respectively, for the electric current density, Maxwell stress tensor (MST), electric field, electric displacement, electrical conductivity, permittivity, electric potential, and total electric current density. The second stage of the algorithm is the calculation of the mechanical part, based on

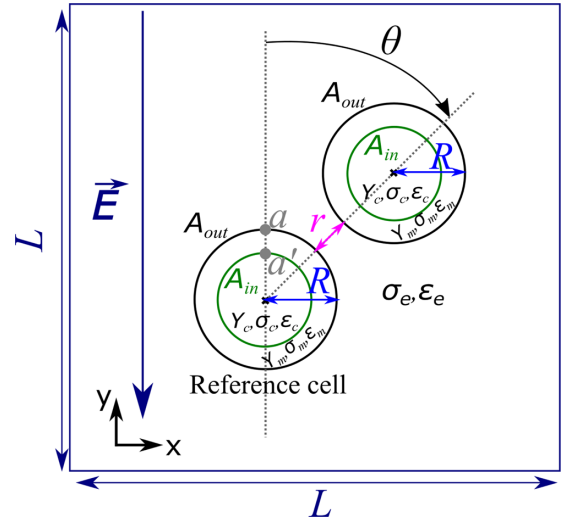


FIG. 1. Schematic of a typical square computational domain filled with the ECM to study the amplitude of the MST at point  $a'$ . The two cells are initially separated by distance  $r$  (not to scale). The orientation angle denoted by  $\theta$  refers to the angle of the line joining the cell centers of mass relative to the electric field direction applied along the  $y$  direction. Right and left boundaries are insulated while the top and bottom walls are prescribed with an applied potential. Dirichlet boundary conditions at the top and bottom boundaries are justified as the electric field is applied through discrete electrodes;  $a$  and  $a'$  define the points on the outer and inner layer of the cell membrane allowing us to calculate the TMP at the pole. Surface charge distributions of  $\pm 6.2 \times 10^{-4} \text{ C m}^{-2}$  were added to both surfaces  $A_{in}$  and  $A_{out}$  in order to account for a resting potential of  $-70 \text{ mV}$ .

the outputs of the previous stage:  $\nabla \cdot \mathbf{S} + \mathbf{F} = -\rho(\partial^2 \mathbf{u} / \partial t^2)$ ,  $\mathbf{S} = \mathbf{C} \cdot \boldsymbol{\kappa}$ , and  $\boldsymbol{\kappa} = \frac{1}{2} [\nabla(\mathbf{u})^T + (\nabla \mathbf{u})]$ , where  $\mathbf{F}$ ,  $\mathbf{S}$ ,  $\mathbf{C}$ ,  $\boldsymbol{\kappa}$ ,  $\rho$ ,  $t$ , and  $\mathbf{u}$  account, respectively, for external volume force, stress tensor, compliance tensor, strain tensor, density, time, and displacement vector. It is worth observing that the acceleration term  $\rho(\partial^2 \mathbf{u} / \partial t^2)$  in the momentum equation can be neglected since the viscous relaxation time is faster than the changes in the applied electric field [1].

The cells are subjected to an AC electric field and we assume that the nonuniformity of this field is modest on the scale of the cell's dimension. As we see, physics can depend very strongly on  $V_m$ , which is computed by subtracting the cytoplasm-membrane interface potential ( $V_{m-in}$ ) to the membrane-extracellular medium interface potential ( $V_{m-out}$ ), i.e.,  $V_m = V_{m-out} - V_{m-in}$ . Here we are only interested at the TMP at the pole  $V_{maa'}$  for the reference cell displayed in Fig. 1. Also note that we assume a resting potential  $V_{rest}$  set to  $-0.07 \text{ V}$  which is constant everywhere on the cell membrane [2,10]. When an external electric field  $E$  is applied to the cell the TMP  $V_m$  superimposes to  $V_{rest}$ . Observe that  $V_m$  tends to  $V_{rest}$  when  $\nu$  is much greater than  $\nu_\beta$  (Fig. 1). Let us now introduce what exactly is meant by MST. The frequency dependent excess MST is defined at point  $a'$  of Fig. 1 and reads  $\frac{MST(\nu)_{1cell} - MST(\nu)_{2cells}}{MST(\nu=10 \text{ Hz})_{1cell}}$ , where subscripts "1cell" and "2cells," respectively, correspond to the single-cell and two-cell configurations.

This system has recently been mathematically modeled [9], as a step toward the understanding of mechanobiology into

a quantitative, predictive model of the events linking ED to electroporation. The most relevant result for us is the electric field anisotropy which is described by the orientation angle denoted by  $\theta$ . This parameter refers to the angle of the line joining the cell centers of mass relative to the electric field direction applied along the  $z$  direction. The material parameter values for the membrane thickness of the undeformed cell is  $d_{m0} = 5$  nm, cell radius (in the undeformed state)  $R = 5 \mu\text{m}$ , membrane conductivity  $\sigma_m = 5 \times 10^{-7} \text{ S m}^{-1}$ , membrane permittivity  $\varepsilon_0 \varepsilon_m = 4.4 \times 10^{-11} \text{ F m}^{-1}$ , cytoplasm conductivity  $\sigma_c = 0.2 \text{ S m}^{-1}$ , cytoplasm permittivity  $\varepsilon_0 \varepsilon_c = 7 \times 10^{-10} \text{ F m}^{-1}$ , ECM conductivity  $\sigma_e$  ranging from  $0.013$  to  $2 \text{ S m}^{-1}$ , ECM permittivity  $\varepsilon_0 \varepsilon_e = 7 \times 10^{-10} \text{ F m}^{-1}$ , membrane Young's modulus  $Y_m = 19 \text{ MPa}$ , and cytoplasm Young's modulus  $Y_c = 100 \text{ Pa}$  [9]. Here the Poisson ratio of the cytoplasm and membranes are set to  $0.4$  and  $0.49$ , respectively [11]. The cytoplasm is characterized by a complex (relative) permittivity  $\varepsilon_c(\nu) = \varepsilon_c + \sigma_c / (2\pi i \varepsilon_0 \nu)$  covered by a confocal membrane characterized by a complex (relative) permittivity  $\varepsilon_m(\nu) = \varepsilon_m + \sigma_m / (2\pi i \varepsilon_0 \nu)$  suspended in a continuous ECM characterized by a (relative) permittivity  $\varepsilon_e(\nu) = \varepsilon_e + \sigma_e / (2\pi i \varepsilon_0 \nu)$ . Here,  $\varepsilon_0$  is the permittivity of free space. The two cells are separated by a distance  $r/R = 0.2$ , i.e., a choice which is motivated from our study of separation distance–orientation angle diagrams; we include a discussion of the influence of this parameter on the ED force distribution in the Supplemental Material [20]. The cells are subjected to an electric field for a given amplitude set to  $0.815 \text{ kV cm}^{-1}$ .

Five comments are in order. (1) The overall membrane width is variably reported to be anywhere between  $4$  and  $10$  nm due to the numerous types of lipids and proteins. A value in the range  $4$ – $5$  nm is most representative of the membrane shaved off from its outer and inner protrusions. Furthermore, the bilayer thickness of the membrane is critical in hydrophobic matching and it has been suggested that cholesterol is the principal modulator of bilayer thickness in eukaryotic cells. The standard value used in most numerical simulations dealing with model membranes exposed to electric fields is  $5$  nm in the archival literature [3–4,9–14,19,21]). (2) In some cases in-plane ordering, especially in highly and anisotropically curved membrane regions, might suggest properties that have the potential to affect vesicle shape but geometrical constructions of the type presented in [22] need some refinement to be viable under electric field excitation. (3) When considering a membrane as a 2D object its mechanical properties in the absence of anisotropies can be characterized by the Young's modulus and the Poisson's ratio according to continuum elasticity theory. In the archival literature, neither Young's modulus nor Poisson's ratio have been determined separately so far (even if the Young's modulus and Poisson's ratio are interrelated by a formula that incorporates the bending rigidity [23]). The Poisson's ratio in the gel phase of a coarse grained lipid membrane model has been found to be close to  $0.5$  [24]. The analysis of volume compressibility of lipid membranes within the framework of linear elasticity theory for homogeneous thin fluid sheets shows that lipid membrane deformations are to a very good approximation volume preserving, with a Poisson ratio that is likely about  $3\%$  smaller than the common soft matter limit  $0.5$  [25]. (4) One of the basic assumptions (limitations) of our study

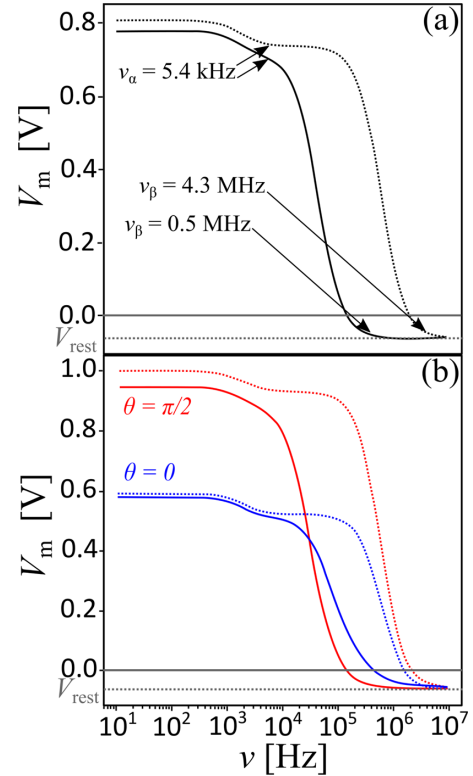


FIG. 2. (a) TMP at the pole for the reference single cell as a function of frequency of the electric field. Solid (resp., dotted) lines correspond to  $\Lambda$  set to  $15$  (resp.,  $0.1$ ); (b) as in (a) for the two-cell configuration (Fig. S1 [20]). Blue (resp., red) lines correspond to  $\theta = 0$  (resp.,  $\theta = \pi/2$ ).

is to consider linear, homogeneous, and isotropic membranes and cytoplasm. In point of fact, our next goal will be to apply these simulation tools to deal with  $\mu\text{s}$  and sub- $\mu\text{s}$  electroporation for which the cross-membrane transport and the local electrical properties are central, and linear mechanical behavior can be safely assumed due to force amplitudes and shortness of the considered timescales [26,27]. Within this perspective, it is known that when the TMP exceeds a certain value, hydrophilic membrane pores greater than a particular size become favorable because they provide lower energy states than the intact lipid bilayer which holds otherwise more capacitive energy. (5) One should keep in mind that the electrical timescales are several orders of magnitude smaller than the viscous relaxation time. Thus, based on the decoupling of the electric and hydrodynamic equations, our algorithm solves a set of equations within the scope of quasistatic mechanical equilibrium [28].

### III. RESULTS AND DISCUSSION

Our results are discussed from three perspectives. Firstly, we examine the impact of conductivity ratio  $\Lambda$  on TMP at the pole. We display two different choices of  $\Lambda$ , corresponding to increasing or decreasing  $\sigma_e$  and  $\sigma_c$  is constant. We present our results in Fig. 2 as a function of frequency for the single-cell case. For a single-cell configuration, TMP can be expressed as  $V_m(\omega, t, \psi) = \frac{3}{2} \frac{RE_0}{\sqrt{1+\omega^2\tau^2}} \cos(\psi) \cos[\omega t - \arctan(\omega\tau)]$ , where

$E_0$ ,  $\psi$  and  $\tau$ , respectively, account for the magnitude of the exogenous field, the angle between the electric field direction and position on the membrane contour, and the membrane charging time defined as  $\tau = RC_m(\frac{1}{\sigma_c} + \frac{1}{2\sigma_a})$ ,  $C_m$  denoting the membrane capacitance [28]. In Fig. 2, we display the location of  $\nu_\alpha$  and  $\nu_\beta$  by arrows with corresponding relaxation times  $\tau_\alpha \sim 1$  ms and  $\tau_\beta \sim 0.1$   $\mu$ s, respectively. The top panel of Fig. 2 depicts the strong decrease in TMP for a single cell, as the frequency is increased from kHz to several MHz, in accordance with earlier results [1,29]. We observe a blueshift of  $V_m$  at the  $\beta$ -dispersion frequency when the conductivity of the ECM is increased. This is due to the fact that if the intracellular medium is more conductive than the ECM, the cell is more polarizable than the medium. Complementary results (not shown) indicate a blueshift of the  $\alpha$ -dispersion frequency in the graph of  $V_m$  as the membrane conductivity is increased. This observation is consistent with a higher tangential mobility of ions on the membrane surface decreasing the associated characteristic dispersion timescale and shifting the value of  $\nu_\alpha$  toward higher frequency value [1]. The bottom panel of Fig. 2 displays the TMP corresponding to the two-cell case. Asymmetry is always important at low frequencies,  $\nu < \nu_\alpha$ , since Fig. 2 shows a 24% increase (resp., 27% decrease) in the magnitude of  $V_m$  when the two cells are aligned (resp., perpendicular) with the electric field direction in accordance with the fact that the membrane represents a barrier limiting the polarization of the intracellular medium at low frequencies [4]. However, evidence suggests that at higher frequencies,  $\nu > \nu_\beta$ ,  $V_m$  changes abruptly with a noticeable blueshift of the displacement of the  $V_m$  decay for a large conductivity ratio. Overall, these results show the extreme sensitivity of proximity-induced capacitive coupling arising concomitantly when the magnitude of the ED force increases as the distance between cells is decreased (see Supplemental Material [20]) and the spatial anisotropy becomes important.

Secondly, because TMP is only a single parameter, it is likely that the true richness of ED can be fully appreciated by considering the MST driving cytoplasmic remodeling under electric field excitation. An exciting result bearing on this issue is the frequency-sensitive modulation of the ED force induced by the local TMP: At low frequencies,  $\nu < \nu_\alpha$  Fig. 3 shows that there is a 47% decrease (resp., 53% increase) in the magnitude of  $F_{ED}$  when the two cells are aligned (resp., perpendicular) with the electric field direction while at high frequencies,  $\nu > \nu_\beta$ , the ED force profile shifts to progressively higher frequencies as  $\Lambda$  is decreased.

Upon further inspection, our results quantitatively confirm the quadratic variation of the MST as a function of  $V_m$  (not shown) and its dependence on variations in proximity factor  $r/R$  as reported in the Supplemental Material [20]. Additionally, our work also indicates that the elastic fields emanating from the Maxwell stress tensor are highly localized (Fig. 4).

Upon application of an electric field energy redistributes to maintain consistent boundary conditions through a perturbation of line fields for the single-cell and two-cell configurations. Notice that Fig. 4 reinforces the trend shown in Figs. 2 and 3 indicating that the frequency of the applied electric field controls the modulation of electrical cues and ED force. Comparing these results for the single-cell configuration at two values of  $\Lambda$  and fixed frequency [Fig. 4(a)]

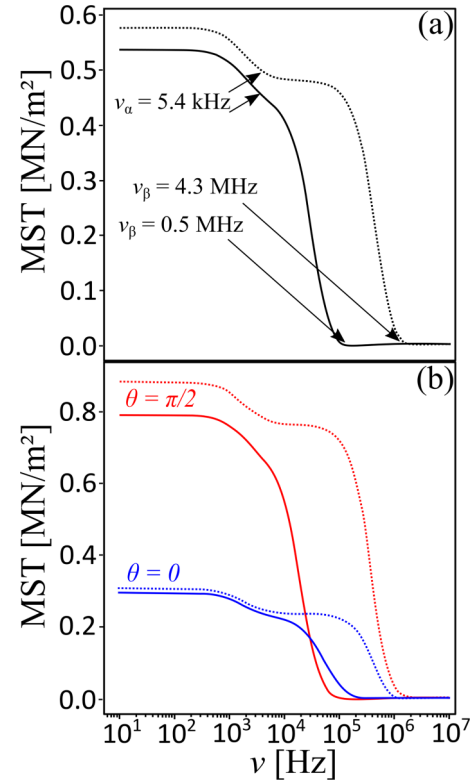


FIG. 3. (a) MST at the pole for the reference single cell as a function of frequency of the electric field. Solid (resp., dotted) lines correspond to  $\Lambda$  set to 15 (resp., 0.1); (b) as in (a) for the two-cell configuration (Fig. S1 [20]). Blue (resp., red) lines correspond to  $\theta = 0$  (resp.,  $\theta = \pi/2$ ).

with the evolution of the aspect ratio (defined as the ratio of semimajor axis  $b$  to semiminor axis  $a$  of the ellipsoid) of the cell deformation induced by the electric field as a function of frequency [left panel of Fig. 4(b)] indicates that shape anisotropy has a much weaker influence on ED of the cell membrane compared to the anisotropy induced by the orientation angle itself. Notice that the decrease of the aspect ratio beyond the  $\alpha$ -dispersion frequency is consistent with the slight reduction in the intensity of the MST shown in Fig. 2 resulting in a decrease of the deformation. Furthermore, one sees explicitly in the left panel of Fig. 4(b) a minimum of the aspect ratio as the field frequency approaches the  $\beta$ -dispersion frequency when  $\Lambda < 1$ . This is due to the frequency dependent sign inversion of the local net electric field imbalance across the membrane (which is the main driver behind the reduction of its local absolute value and thereby of the local intensity of the MST), occurring for a more polarizable ECM than the cytoplasm. We observe in the right panel of Fig. 4(b) how the deformation of the reference cell for a two-cell configuration and anisotropy impacts electromechanical coupling compared to the single-case configuration. Interestingly, the two cases ( $\theta = \pi/2$  and  $\Lambda = 0.1$ ;  $\theta = 0$  and  $\Lambda = 15$ ) considered in Fig. 4(b) suggest that sensitive tuning of the mutual attraction between cells can be achieved at particular orientations of the cells to the field direction, with varying both  $\Lambda$  and frequency.

It is also informative to discuss our results with those dealing with the ED of a single (quasispherical in the unde-

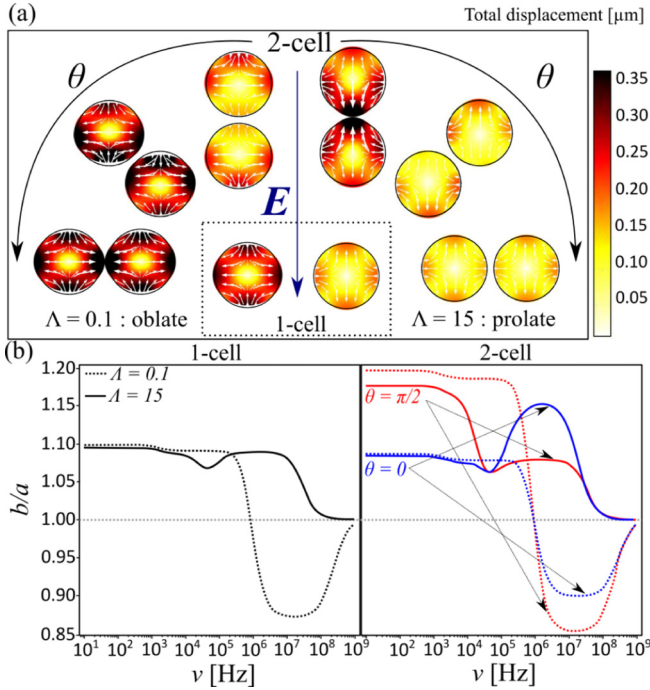


FIG. 4. (a) Effect of increasing the rotation angle  $\theta$  on the local distribution of the cell displacement arising from ED forces for the single-cell and two-cell configurations. The electric field is vertically oriented and frequency is fixed to 10 MHz. White arrows represent the direction of the local displacement field and the color bar shows the total displacement. (b) Evolution of the deformation induced by the electric field in terms of the aspect ratio  $b/a$  (defined as the ratio of semimajor axis  $b$  to semiminor axis  $a$  of the ellipsoid) as a function of frequency of the electric field. The solid and dotted lines correspond to  $\Lambda = 15$  and  $\Lambda = 0.1$ , respectively, while the red and blue curves correspond to values of  $\theta$  set to  $\pi/2$  and 0, respectively. Black arrows are guides to the eye for the curves associated with different values of  $\theta$ .

formed state) giant unilamellar vesicle in AC electric fields; see, e.g., Refs. [1,16]. One main difference between the two studies is that the inner media (cytoplasm) is described via the continuum elasticity theory rather than fluid mechanics. Despite such difference, we see similar trends of the ellipsoidal deformation in uniform alternating electric field as a function of the frequency due to the decoupling of the electric and hydrodynamic modeling. Varying the ECM conductivity can induce morphological deformations, i.e., prolate-oblate transitions as a function of  $\Lambda$  and frequency which closely resemble those displayed in Fig. 4(b). Since the cytoplasm's mechanical behavior is described by an elastic modulus which is five orders of magnitude lower than that of the membrane, and because the membrane thickness is three orders of magnitude smaller compared to the cell's radius, increasing  $Y_c$  by one order of magnitude induces an increase of the effective modulus of the core(cytoplasm)-shell(membrane) system (and consequently, its resistance to deformation) thereby producing a significant impact on the amplitude of deformation induced by the electric field leading to a reduction of the aspect ratio and the amplitude of the total displacement by two orders of magnitude (see Supplemental Material [20]).

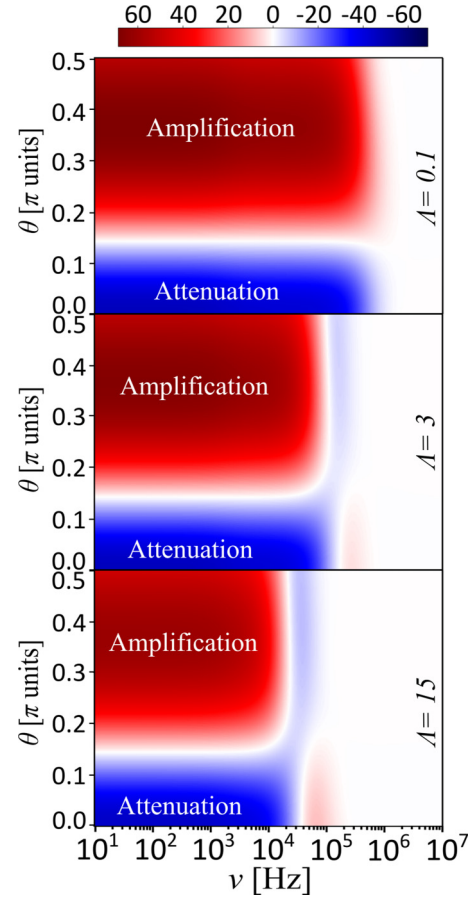


FIG. 5. Characterizing the anisotropy of the attenuation-amplification transition of the excess MST taken at the pole of the reference cell as a function of frequency of the electric field for values of  $\Lambda$  ranging from 0.1 (bottom) to 15 (top). The color bar represents the excess MST at the pole of the reference cell in percent. The blue and red regions correspond, respectively, to attenuating and amplifying proximity effect induced by the presence of the neighboring cell. A cubic spline interpolation algorithm in the PYTHON programming language was used to plot the diagram. The simulation data on the  $y$  axis correspond to values of  $\theta = i(\pi/10)$ , with  $i = 0, \dots, 5$  and data on the  $x$  axis were logarithmically sampled at a rate of eight points per decade.

Our results are also in accordance with the analytical calculations reported by Ye [30] showing that a vesicle under DC electric field excitation ( $2 \text{ kV cm}^{-1}$ ) exhibits similar trends in prolate-oblate deformation transitions, and where decreasing membrane conductivity of a few orders of magnitude can result in oblate geometries when the ECM is more conductive than the cytoplasm.

Thirdly, to investigate the implication of the anisotropy induced by the orientation angle on the MST distribution we present the evolution of the frequency dependent attenuation-amplification transition of the excess MST taken at the pole of the reference cell (point  $a'$  in Fig. 1) in Fig. 5.

Such frequency-orientation angle diagram allows us to determine the attenuation-amplification transition of the MST at a given value of the proximity factor  $r/R$ . As was shown in [9], lower (resp., larger) values of  $\theta$  tend to favor attenuation (resp., amplification) of the excess MST for a pair of cells

compared to the MST for a single cell in the low frequency ( $\nu < \nu_\omega$ ) regime. Frequency has a significant impact on the transitional behavior for a large value of the conductivity ratio  $\Lambda$  suggesting that shape anisotropy has an even weaker influence on ED of the cell membrane compared to the anisotropy induced by the orientation angle when considering intracellular conditions of greater electrical polarizability than those of the ECM. When we dial the angle  $\theta$  toward a critical value from either side of the frequency-orientation angle diagram the behavior of the attenuation-amplification transition of ED force diverges. This latter property makes the ED force the most interesting parameter for applications as it allows confinement and manipulation of cells using alternating electric fields.

#### IV. CONCLUSION AND OUTLOOK

To summarize, the calculations reported here are intended to show that a simple continuum model of cells suspended in a fluid medium can generate sizable contributions to local MST distribution. The key point to take away from this study is that the modulation of electrical cues and MST by the frequency (from hundreds of kHz to tens of MHz) of the applied electric field provides an extremely rich tool kit for manipulating cells. Our model provides evidence that shape anisotropy has a much weaker influence on ED of the cell membrane compared to the anisotropy induced by the orientation angle itself. The behaviors of the attenuation-amplification transition of MST in a frequency-orientation angle diagram could not have been anticipated without detailed calculation. Measuring physical and in particular biomechanical properties at a single-cell-scale level is a difficult and often challenging task [31]. Our results provide several testable hypotheses of how membrane polarization functions in a variety of cellular shapes involving ED. At least in principle, the above-mentioned differences in

MST distribution illustrated in Fig. 3 might be exploited to create mechanical-based targeting strategies for discriminating between tumor and healthy cells, since the former are about 70% softer than the latter [32].

The question of how mechanotransduction events involving the cell nucleus, cytoskeleton, elastic membrane, and cytosol act on the ED cell behavior remains substantially an open issue, i.e., conversion of ED force into biochemical signals [33]. Controlling frequency and polarization of electromagnetic waves is key for a full manipulation of cell interactions. This dynamical study offers the hope of a complete and accurate method to describe the mechanical force field in multicellular structures induced by an electric stimulation. Ultimately, it is experiments that will hopefully shed light on the precise nature of the cell membrane ED and bioelectric cues. The latter are expected to find important applications in structures on several scales (from single cells to tissues), and provide a quantitative assessment of the role of elastic interactions among a set of cells on their effective electric field induced mechanical behavior. While we limit our study to a pair of cells we anticipate that the work will open a window into the emergent mechanobiology techniques for confinement, manipulation, and actuation of biological materials using electric fields [34].

The data that support the findings of this study are available from the corresponding author upon reasonable request.

#### ACKNOWLEDGMENTS

E.S. would like to thank Université de Brest for supporting this research through its Ph.D. program. This work was performed under the auspices of the Lab-STICC which is the Unité Mixte de Recherche CNRS 6285.

- 
- [1] K. A. Riske and R. Dimova, Electro-deformation and poration of giant vesicles viewed with high temporal resolution, *Biophys. J.* **88**, 1143 (2005); P. M. Vlahovska, R. Serral Gracià, S. Aranda-Espinoza, and R. Dimova, Electrohydrodynamic model of vesicle deformation in alternating electric fields, *ibid.* **96**, 4789 (2009).
  - [2] K. R. Foster and H. P. Schwan, Dielectric properties of tissues and biological materials: A critical review, *Crit. Rev. Biomed. Eng.* **17**, 25 (1989).
  - [3] K. Asami, Dielectric dispersion in biological cells of complex geometry simulated by the three-dimensional finite difference method, *J. Phys. D: Appl. Phys.* **39**, 492 (2006); Characterization of heterogeneous systems by dielectric spectroscopy, *Prog. Polym. Sci.* **27**, 1617 (2002).
  - [4] M. Essone Mezeme and C. Brosseau, Simulation of a toy model of cylindrical cells submitted to nonionizing electromagnetic field: Effect of membrane cell disruption, *J. Appl. Phys.* **107**, 014701 (2010); Time-varying electric field induced transmembrane potential of a core-shell model of biological cells, **108**, 014701 (2010); A. Di Biasio, L. Ambrosone, and C. Cametti, The dielectric behavior of nonspherical biological cell suspensions: An analytic approach, *Biophys. J.* **99**, 163 (2010).
  - [5] J. Gimsa and D. Wachner, A polarization model overcoming the geometric restrictions of the Laplace solution for spheroidal cells: Obtaining new equations for field-induced forces and transmembrane potential, *Biophys. J.* **77**, 1316 (1999).
  - [6] G. Bryant and J. Wolfe, Electromechanical stresses produced in the plasma membranes of suspended cells by applied electric fields, *J. Membr. Biol.* **96**, 129 (1987).
  - [7] M. Kummrow and W. Helfrich, Deformation of giant lipid vesicles by electric fields, *Phys. Rev. A* **44**, 8356 (1991).
  - [8] V. Sukhorukov, H. Mussauer, and U. Zimmermann, The effect of electrical deformation forces on the electroporation of erythrocyte membranes in low- and high-conductivity media, *J. Membr. Biol.* **163**, 235 (1998).
  - [9] E. Sabri and C. Brosseau, Proximity-induced electrodeformation and membrane capacitance coupling between cells, *Eur. Biophys. J.* **50**, 713 (2021).

- [10] C. Brosseau and E. Sabri, Resistor-capacitor modelling of the cell membrane: A multiphysics analysis, *J. Appl. Phys.* **129**, 011101 (2021).
- [11] D. Shamoon, J. Dermol-Cerne, L. Rems, M. Rebersek, T. Kotnik, S. Lasquellec, C. Brosseau, and D. Miklavčič, Assessing the electro-deformation and electro-permeabilization of biological cells using a three dimensional finite element model, *Appl. Phys. Lett.* **114**, 063701 (2019); D. Shamoon, S. Lasquellec, and C. Brosseau, A multiphysics analysis of the strain energy in multicellular environments, *ibid.* **115**, 043701 (2019); F. Guo, K. Qian, H. Deng, and X. Li, Multiphysics analysis of nsPEF induced electrodeformation in a dispersive cell model, *ibid.* **118**, 083701 (2021).
- [12] E. Sabri, S. Lasquellec, and C. Brosseau, Electromechanical modeling of the transmembrane potential-dependent cell membrane capacitance, *Appl. Phys. Lett.* **117**, 043701 (2020).
- [13] A. Morshed, P. Dutta, M. R. Hossan, and R. Dillon, Electrodeformation of vesicles suspended in a liquid medium, *Phys. Rev. Fluids* **3**, 103702 (2018).
- [14] H. Nganguia and Y. N. Young, Equilibrium electrodeformation of a spheroidal vesicle in an ac electric field, *Phys. Rev. E* **88**, 052718 (2013).
- [15] S. Aranda, K. A. Riske, R. Lipowsky, and R. Dimova, Morphological transitions of vesicles induced by alternating electric fields, *Biophys. J.* **95**, L19 (2008).
- [16] P. Peterlin, Frequency-dependent electrodeformation of giant phospholipid vesicles in AC electric field, *J. Biol. Phys.* **36**, 339 (2010).
- [17] E. C. Gianulis, M. Casciola, S. Xiao, O. N. Pakhomova, and A. G. Pakhomov, Electroporation by uni- or bipolar nanosecond electric pulses: The impact of extracellular conductivity, *Bioelectrochem.* **119**, 10 (2018); T. Kotnik, G. Pucihar, and D. Miklavčič, The cell in the electric field, in *Clinical Aspects of Electroporation*, edited by S. T. Kee, J. Gehl, and E. W. Lee (Springer Verlag, Berlin, 2011).
- [18] A. Barnett and J. C. Weaver, Electroporation: A unified quantitative theory of reversible electrical breakdown and mechanical rupture in artificial planar bilayer membranes, *Bioelectrochem. Bioenerg.* **25**, 163 (1991); J. C. Weaver, and Y. Chimadzhiev, Theory of electroporation: A review, *ibid.* **41**, 135 (1996).
- [19] E. Goldberg, C. Suarez, M. Alfonso, J. Marchese, A. Soba, and G. Marshall, Cell membrane electroporation modeling: A multiphysics approach, *Bioelectrochemistry* **124**, 28 (2018).
- [20] See Supplemental Material at <http://link.aps.org/supplemental/10.1103/PhysRevE.104.034413> for a description of the material properties of the actual cells which have been deduced from consolidated literature data and additional results.
- [21] COMSOL MULTIPHYSICS version 5.2.
- [22] L. Mesarec, W. Gózdź, A. Iglič, V. Kralj-Iglič, E. G. Virga, and S. Kralj, Normal red blood cells' shape stabilized by membrane's in-plane ordering, *Sci. Rep.* **9**, 19742 (2019).
- [23] E. A. Evans and R. Skalak, *Mechanics and Thermodynamics of Biomembranes* (CRC Press, Boca Raton, FL, 2017).
- [24] T. Jadidi, H. Seyyed-Allaei, M. Reza Rahimi Tabar, and A. Mashaghi, Poisson's Ratio and Young's Modulus of lipid bilayers in different phases, *Front Bioeng Biotechnol.* **2**, 8 (2014).
- [25] M. Mert Terzi, M. Deserno, and J. F. Nagle, Mechanical properties of lipid bilayers: A note on the Poisson ratio, *Soft Matter* **15**, 9085 (2019); W. Chen, F. Duša, J. Witos, S. K. Ruokonen, and S. K. Wiedmer, Determination of the main phase transition temperature of phospholipids by nanoplasmonic sensing, *Sci. Rep.* **8**, 14815 (2018).
- [26] E. Moeendarbary, L. Valon, M. Fritzsche, A. R. Harris, D. A. Moulding, A. J. Thrasher, E. Stride, L. Mahadevan, and G. T. Charras, The cytoplasm of living cells behaves as a poroelastic material, *Nat. Mater* **12**, 253 (2013).
- [27] J. Eid, H. Greige-Gerges, L. Monticelli, and A. Jraij, Elastic moduli of lipid membranes: Reproducibility of AFM measures, *Chem. Phys. Lipids* **234**, 105011 (2021).
- [28] P. M. Vlahovska, Nonequilibrium dynamics of lipid membranes: Deformation and stability in electric fields, in *Advances in Planar Lipid Bilayers and Liposomes* (Elsevier, Amsterdam, 2010), Vol. 12, pp. 101–146.
- [29] C. Holzapfel, J. Vienken, and U. Zimmermann, Rotation of cells in an alternating electric field: Theory and experimental proof, *J. Membr. Biol.* **67**, 13 (1982).
- [30] H. Ye, Kinematic difference between a biological cell and an artificial vesicle in a strong DC electric, *BMC Biophysics* **10**, 6 (2017).
- [31] N. Guz, M. Dokukin, V. Kalaparthi, and I. Sokolov, If cell mechanics can be described by elastic modulus: Study of different models and probes used in indentation experiments, *Biophys. J.* **107**, 564 (2014).
- [32] O. Chaudhuri and D. J. Mooney, Stem cell differentiation: Anchoring cell-fate cues, *Nat. Mater.* **11**, 568 (2012); M. Fraldi, A. Cugno, L. Deseri, K. Dayal, and N. M. Pugno, A frequency-based hypothesis for mechanically targeting and selectively attacking cancer cells, *J. R. Soc. Interface* **12**, 20150656 (2015).
- [33] P. A. Janmey and C. A. McCulloch, Cell mechanics: Integrating cell responses to mechanical stimuli, *Annu. Rev. Biomed. Eng.* **9**, 1 (2007); C. T. Lim, E. H. Zhou, and S. T. Quek, Mechanical models for living cells: A review, *J Biomech.* **39**, 195 (2006).
- [34] J. Arnadóttir and M. Chalfie, Eukaryotic mechanosensitive channels, *Annu. Rev. Biophys.* **39**, 111 (2010).